NIH Public Access
Author Manuscript
Biomed Microdevices. Author manuscript; available in PMC 2011 June 1.

Published in final edited form as:
Biomed Microdevices. 2010 June ; 12(3): 533–541. doi:10.1007/s10544-010-9410-9.

Droplet-based microsystem for multi-step bioreactions

Fang Wang and
Department of Chemical Engineering, University of Michigan, Ann Arbor, MI 48109, USA

Mark A. Burns
Department of Chemical Engineering, University of Michigan, Ann Arbor, MI 48109, USA

Department of Biomedical Engineering, University of Michigan, Ann Arbor MI 48109 USA

Mark A. Burns: maburns@umich.edu

Abstract

A droplet-based microfluidic platform was used to perform on-chip droplet generation, merging and mixing for applications in multi-step reactions and assays. Submicroliter-sized droplets can be produced separately from three identical droplet-generation channels and merged together in a single chamber. Three different mixing strategies were used for mixing the merged droplet. For pure diffusion, the reagents were mixed in approximately 10 min. Using flow around the stationary droplet to induce circulatory flow within the droplet, the mixing time was decreased to approximately one minute. The shortest mixing time (10 s) was obtained with bidirectional droplet motion between the chamber and channel, and optimization could result in a total time of less than 1 s. We also tested this on-chip droplet generation and manipulation platform using a two-step thermal cycled bioreaction: nested TaqMan® PCR. With the same concentration of template DNA, the two-step reaction in a well-mixed merged droplet shows a cycle threshold of ~6 cycles earlier than that in the diffusively mixed droplet, and ~40 cycles earlier than the droplet-based regular (single-step) TaqMan® PCR.

Keywords

Droplet; Microfluidics; Merging; Mixing; Nested PCR

1 Introduction

Over the past decade, microfluidic formation of liquid droplets in a second liquid phase has found many applications in chemical and biochemical reactions and assays (Beer et al. 2007, 2008; Chabert and Viovy 2008; Huebner et al. 2007; Hung et al. 2006; Kumaresan et al. 2008; Mohr et al. 2007; Ohashi et al. 2007; Schaerli et al. 2009; Srisa-Art et al. 2007; Zheng et al. 2004). The size and generation frequency of these droplets are mostly controlled by adjusting the flow rates and channel geometry of the microfabricated device (Anna et al. 2003; Thorsen et al. 2001). In electrowetting-on-dielectric (EWOD) systems, the control is performed by electronically changing the interfacial energy (Cho et al. 2003; Pollack et al. 2000, 2002). Splitting, merging and sorting of droplets have also been achieved using these control methods (Chabert and Viovy 2008; Hung et al. 2006; Link et al. 2004; Niu et al.

© Springer Science+Business Media, LLC 2010

Correspondence to: Mark A. Burns, maburns@umich.edu.

Electronic supplementary material The online version of this article (doi:10.1007/s10544-010-9410-9) contains supplementary material which is available to authorized users.

NIH-PA Author Manuscript
NIH-PA Author Manuscript
NIH-PA Author Manuscript

NIH-PA Author Manuscript

NIH-PA Author Manuscript

NIH-PA Author Manuscript

2008; Sarrazin et al. 2007; Tan et al. 2004; Ting et al. 2006; Um and Park 2009). Other driving sources for droplet generation and manipulation have been used such as dielectrophoresis (DEP) (Ahmed and Jones 2006; Jones 2001), surface acoustic wave (SAW) (Guttenberg et al. 2005; Franke et al. 2009) and magnetic force (Lehmann et al. 2006; Pipper et al. 2007). Relying on the controllable two-phase microfluidics, the droplet-based microsystems offer advantages in reducing and isolating reaction volumes, preventing evaporation and adsorption, and improving mixing and reaction efficiencies.

Controllable droplet merging and mixing are crucial to successfully performing chemical and biochemical reactions in the droplets, and both passive and active methods have been developed. In passive droplet merging, the drainage of the continuous phase between two droplets is promoted by changing the channel geometry or adding channel structures (Hung et al. 2006; Niu et al. 2008; Sarrazin et al. 2007; Tan et al. 2007; Um and Park 2009). Active droplet merging can be achieved by actively guiding the droplets towards each other in EWOD (Cho et al. 2003), SAW (Guttenberg et al. 2005) or magnetic-based (Lehmann et al. 2006; Pipper et al. 2007) systems. As is known, diffusive mixing is dominant in microscale and can be excessively slow in spite of the short diffusion distances. In a droplet-based microsystem, mixing can be accelerated using passive methods by flowing the droplets through certain shaped channels to induce internal circulation and chaotic advection (Bringer et al. 2004; Handique and Burns 2001; Rhee and Burns 2008; Sarrazin et al. 2007; Song et al. 2003). In EWOD, SAW and magnetic-based droplet systems, mixing can also be completed by actively moving the droplets along a certain path (Guttenberg et al. 2005; Lehmann et al. 2006; Paik et al. 2003; Pipper et al. 2007).

Droplet-based microsystems integrated with droplet merging and mixing are ideal for chemical and biochemical applications that require controllable addition of reagents, for example, in aggressive or fast reaction and kinetic studies (Frenz et al. 2008; Guttenberg et al. 2005; Hung et al. 2006; Pipper et al. 2007; Srinivasan et al. 2004). These systems are also highly amenable to multi-step reactions. In fact, many bioassays include more than one reaction step. However, only synthesis of core-shell nanoparticles has been reported using a droplet-based two-step reaction (Shestopalov et al. 2004). Moreover, most droplet-based applications use small (e.g., picoliter-sized) droplets, but nano-to microliter droplets still need to be employed in cases where target molecules with very low concentration need to be detected (Avettand-Fènoël et al. 2009; Sivapalasingam et al. 2007). Passive mixing strategies employed in previous works may not be practical in these large droplets since the mixing channel needs to be very long (Handique and Burns 2001), thus increasing the device size. In addition, chaotic advection may not enhance mixing in these long, plug-shaped droplets because the striation is only formed in the front half of the plug (Bringer et al. 2004). Therefore, alternative mixing strategies need to be explored for applications involving large droplets.

In this paper, we present studies on droplet merging and mixing in a microfluidic platform for multi-step biochemical reactions. Submicroliter-sized droplets generated separately from three different channels can easily merge together in a central chamber. The chamber also serves as a compartment for conducting mixing and reactions. Different mixing strategies have been studied to enhance mixing in the merged droplet. Furthermore, we demonstrate the application of this droplet-based platform by performing nested TaqMan® PCR, a two-step bioreaction, with on-chip droplet generation, merging and mixing.

2 Materials and methods

2.1 Device design and fabrication

The entire fluid network is 100 μm deep. Most the microchannels are 400 μm wide except that the neck region following the slanted T-junction is 220 μm wide and channels C1 and C4 (Fig.

NIH-PA Author Manuscript

NIH-PA Author Manuscript

NIH-PA Author Manuscript

1(a)) in the device for mixing with bidirectional droplet motion are 800 μm wide. Each side of the diamond chamber is ~1690 μm long. The fabrication procedure for the fluid network has been outlined in details elsewhere (Pal et al. 2005). Briefly, a thin metal film (500Å Cr/ 2500Å Au) is deposited and patterned on a glass wafer. The glass wafer is then etched to the desired depth in 49% hydrofluoric acid (CMOS grade; J.T. Baker, Philipsburg, NJ). Next, the photoresist and the metal layer are removed. The glass wafer is then diced to obtain individual dies. The dies are coated with a 3 μm thick layer of Parylene-C (PDS 1020 Labcoater, Speciality Coating Systems, IN) before bonded to the bottom dies.

Four sets of heaters and resistance temperature detectors (RTDs) on each die are fabricated on a silicon wafer with a 5000Å thick silicon oxide layer. Firstly, photoresist is patterned on the silicon wafer using photolithography. Next, 300Å Ti/ 1000Å Pt is evaporated on the silicon wafer. The wafer is then left in acetone (CMOS grade; J.T. Baker, Philipsburg, NJ) to liftoff unwanted metal. The diced individual silicon dies are fixed on the custom designed printed circuit board (PCB, Advanced Circuits, Aurora, CO), and then wire bonded (Kulicke & Soffa 4124 Ball Bonder) using 1.0 mil gold wire. The assembled silicon die and PCB are also coated with a 3 μm thick layer of Parylene-C. Finally, the glass and silicon dies are visually aligned and then bonded using UV curable optical glue.

2.2 Instrumentation

The setup for on-chip temperature control consists of two data acquisition (DAQ) boards (National instruments PCI 6031E and PCI-6704, Austin, TX), two connector blocks (National instruments SCB-100 and SCB-68, Austin, TX), a signal conditioning circuit, a DC power supply (B+K Precision Model 1760, Yorba Linda, CA), a computer and two LabVIEW programs (National instruments, Austin, TX). One LabVIEW program is used to calibrate the RTDs by recording the temperature-resistance data when the device is heated in a convection oven. The slope and intercept from a linear fit of the temperature and resistance data are read into the control algorithms that use a proportional-integral (PI) module to control temperature. The heaters are connected to the power supply through the signal conditioning circuit that boosts the supply voltage from the computer with an op-amp gain of 3. The precision of temperature control is ±0.2°C. During the experiments, the device is placed on a copper block that sits on a probe station with temperature maintained at 15°C.

Lab air supply serves as the pneumatic source for driving the fluid flow and is controlled using electropneumatic regulators (VSO-EP or VSO-EV; Parker, Cleveland, OH). Pressure or vacuum is applied through syringes connected to each port on the device. The Pulsing of pressure or vacuum is controlled by a set of three-way solenoid valves (Numatech, Wixom, MI). Opening and closing of the solenoid valves are operated through a relay board (Model ER-16; National Instruments, Austin, TX). Functioning of the relay board is controlled in conjunction with a Digital I/O card (National Instrument PCI-DIO-96, Austin, TX) by a LabVIEW program.

2.3 Measurement of micromixing

Aqueous solution with 1.4 g/L fluorescein (Sigma Aldrich, St. Louis, MO) and colorless DI water are used to characterize mixing in the merged droplet. During the mixing process, *in situ* imaging is recorded using a digital camera (Nikon Coolpix 4500) with a capture rate of 30 frames/s. The captured RGB images are converted into grayscale images using Image J (NIH). The grayscale value of each pixel's intensity is processed using a program written in MATLAB (MathWorks, Natick, MA), and the standard deviation $\left(SD=\left\langle (I-\langle I\rangle)^2\right\rangle^{1/2}\right)$ of the droplet area is used to quantify the degree of mixing as described in previous work (Kim et al. 2009). Due to the limitations in our imaging setup, the standard deviation for the unmixed and perfectly

NIH-PA Author Manuscript

NIH-PA Author Manuscript

NIH-PA Author Manuscript

mixed cases is SD_1=0.385 and SD_2=0.1 (instead of the ideal value SD_1=0.5 and SD_2=0), respectively.

2.4 PCR amplification

The reaction mixture for regular TaqMan® PCR consists of λDNA template (Invitrogen, Carlsbad, CA) with the concentration ranging from 3.5 ng/μL to 3.5×10^{-8}ng/μL, 0.2 mM dNTPs, 10 mM Tris-HCl (pH 8.3), 50 mM KCl, 0.01 mM EDTA, 3.5 mM $MgCl_2$, 0.9 μM each primer, 0.25 μM probe, 0.175units/μL AmpliTaq Gold® DNA polymerase (Applied Biosystems, Foster City, CA) and DI H_2O. The sequences of forward and reverse primers are 5'-CATC AAAGCCATGAACAAAGCA-3' and 5'-TCAG CAACCCCGGTATCAG-3', respectively. The sequence of probe is 5'6FAM-CCGCGCTGGATGA-3'MGBNFQA. The size of the target product is 56 bp. The thermal cycling protocol used in the on-chip droplet-based reaction consists of 95°C for 9 min, followed by 16–45 cycles of 95°C for 9 s and 60° C for 30 s. PCR grade mineral oil (Sigma Aldrich, St. Louis, MO) is used as the continuous oil phase.

The reaction mixture for the first-run amplification of nested TaqMan® PCR involves a new set of primers with the concentration of 0.3 μM each. All the other reagents have the same concentrations as in the mixture of regular TaqMan® PCR, except no probe included. The sequences of the new forward and reverse primers are 5'-AACCGA CATGTTGATTTCCT-3' and 5'-AACCTGACTGTTCGA TATATTCACT-3', respectively. The product from the first-run amplification is 112 bp. The thermal cycling protocol used in the on-chip droplet-based reaction consists of 95°C for 9 min, followed by 15 cycles of 95°C for 5 s, 50°C for 15 s and 72°C for 20 s. For the second-run amplification with the TaqMan® probe, the composition of the reaction mixture and the thermal cycling protocol are the same as the regular TaqMan® PCR, except no template DNA included.

2.5 Fluorescence detection of the reaction droplet

The fluorescence of the reaction droplet is monitored using an inverted fluorescence microscope (Nikon Eclipse TE2000-U) with a 2× objective (Nikon). An X-cite Series 120 lamp (EXFO Life Science Divisions, Ontario, Canada) with FITC filter is used as the excitation source. The fluorescence images are captured using a digital CCD camera (Photometrics Cascade 512F; Roper Scientific, Tucson AZ) with a 500 ms exposure time. The relative fluorescence intensity is used to quantify the amplification yield in the droplet, which is calculated by scaling the fluorescence intensity of the droplet by that of the reference area (i.e., the metal heater area) on the device. Data measurement and analysis are done by MetaVue Software. The threshold of the relative fluorescence intensity (1.13) is set manually at the value that the relative fluorescence intensity starts increasing above the background signal. The cycle threshold value (Ct) is determined using interpolation based on the intersection of the fluorescence threshold line and the amplification curve.

3 Results and discussion

3.1 Droplet generation and merging

The device design for droplet generation and merging is shown in Fig. 1(a). There are three identical droplet-generation components each consisting of slanted (45-degree) T-junctions followed by neck regions. Nanoliter-sized droplets with different size and content can be produced from the three components using the sequential injection mode (Wang and Burns 2009). To do this, the entire fluid network is filled with mineral oil by capillary force, and then pulsed pressure (1psig, on for 15 ms, off for 500 ms) is applied to the aqueous phase (Fig. 1 (b)). Once the oil/ aqueous interface reaches the junction, pulsed pressure is applied to both phases to flow the aqueous phase towards the chamber instead of the oil reservoir (Fig. 1(c)).

NIH-PA Author Manuscript

NIH-PA Author Manuscript

NIH-PA Author Manuscript

When the interface reaches the desired position, pressure is only applied to the oil phase to break the aqueous phase into droplet and push the droplet into the chamber while simultaneously pushing the rest of the aqueous phase back to the reservoir (Fig. 1(d)–(e)).

After the droplets are generated, they can be trapped and merged in the central chamber connected to the three droplet generation channel (C1–C3). As shown in Fig. 1(f)–(m) (also Supplementary information, Movie 1), once the first droplet (D1) enters the middle chamber, the pressure that drives the flow is stopped and the surface tension keeps the droplet inside the chamber because of the expanded geometry. Then D1 remains in the chamber and "waits" for the second droplet (D2) to enter the chamber. During the generation and motion of D2, the unblocked channels (C3 and C4) serves as fluid bypass channels to allow the continuous oil phase to flow through. The drainage of the continuous oil phase guides D2 to merge with D1 into a larger droplet (D12). The third droplet (D3) can be generated and merge with D12 using the same method.

There are several advantages in using this device design for applications involving large (nano- to microliter-scale) droplets. The chamber serves as a compartment not only for entrapping and merging droplets, but also for droplet mixing and reaction. This single multi-functional chamber design offers advantages in conservation of device space. Moreover, since the droplet-generation components are connected to the chamber separately, the droplets can be produced either sequentially, as shown above, or synchronously, depending on the application. For example, to carry out a multi-step reaction, reagents for different steps need to be kept separate until the proper conditions are available, so the droplets need to be generated one by one. This design can also be used for small monodispersed droplet-based applications such as high throughput screening, with multiple droplets containing different reactants from and trapped in the same chamber.

3.2 Mixing in the merged droplet

Three major approaches can be used to homogenize a droplet: diffusive mixing, passive mixing and active mixing. Mixing purely by diffusion in the submicroliter merged droplet is excessively slow. As shown in Fig. 2, it took about 10 min to homogenize a merged droplet with a volume of ~200 nL purely by diffusion. In this experiment, fluorescein, with a diffusion coefficient on the order of $10^{-5}cm^2/s$, was used to quantify the mixing. Some reagent molecules (e.g., protein and long-strand DNA) have diffusion coefficients lower than fluorescein by an order of magnitude or more and would thus take even longer to diffusively mix.

Mixing in the droplet can be enhanced by applying pressure through the oil phase in the four channels (C1–C4) while the droplet remains in the chamber (Supplementary information, Movie 2). As above-mentioned, the merged droplet tends to remain inside the expanded chamber because of surface tension. The oil film between the droplet and the top/bottom chamber walls is very thin due to the small chamber depth, so the applied pressure mostly drives the oil phase around the unconfined sides of the droplet. The oil flow shears the oil/water interface and causes internal recirculation in the droplet that results in mixing. This mixing strategy is similar to using internal recirculation by moving the droplet through a channel. As shown in Movie 2 (Supplementary information), when we start applying pressure through the oil phase, the merged droplet deforms to minimize its surface-to-volume ratio and internal recirculation inside the droplet is observed. One thing to be pointed out is that mixing mainly happened in the x–y plane, because the solutes were originally distributed uniformly along the z direction, and the thin oil film between the droplet and the top/bottom chamber walls suppressed shear on those surface and the internal recirculation in that direction.

We have quantified the mixing in the merged droplet with pressure applied in pulsing and continuous modes (Fig. 3). The results show that the droplet can be homogenized within ~65

NIH-PA Author Manuscript

NIH-PA Author Manuscript

NIH-PA Author Manuscript

s using both modes, which is about one tenth the mixing time by diffusion. The results also indicate that mixing using pulsed pressure is slightly faster than using continuous pressure. The reason for this could be related to the presence of non-circulating or static points (i.e., the "dead zones") inside the droplet, especially in large sized droplets (Sarrazin et al. 2007). The recirculation loop cannot reach the "dead zones", so these areas can only mix with the rest of the fluid in the droplet by diffusion. While applying pressure continuously, the recirculation loops and the "dead zones" are relatively constant. In contrast, with pulsed pressure, some chaotic fluid motion may be introduced into droplet, allowing the convective mixing to take place between the loops and the "dead zones".

Another mixing strategy is moving the merged droplet back and forth from the chamber to the channel (Supplementary information, Movie 3). This strategy is similar to the electrically controlled active mixing achieved with droplet oscillating between electrodes in an EWOD device (Paik et al. 2003). As shown in Fig. 4, mixing can be completed much faster (<10 s), compared to mixing with the droplet in the chamber. The result also indicates that the pulsing parameters for the applied pressure in both directions (Table 1) needs to be balanced in order to obtain efficient mixing. For pressure with the same "ON" time in each pulse, the "OFF" time had no significant effect on the mixing efficiency. One thing to be pointed out is that there was a time lag between each pulsing cycle due to the processing speed of the computer program. In addition, although stronger pressure could enhance mixing, if the pressure was too strong (i.e., the pulsing "ON" time is too long and the pulsing frequency is too high), the droplet became unstable and then split while moving back and forth (data not shown).

The bidirectional droplet motion can enhance mixing by increasing the interfacial area between the two miscible fluids. The interfacial area is extended not only by inducing the internal recirculation, but also by stretching the droplet into a long plug while moving it into the channel. For large solute molecules, mixing in the droplet is more likely dispersion-dominated because of the low diffusivity ($D \sim 10^{-6}$–10^{-9} cm^2s^{-1}). Therefore, a long displacement distance is required to complete the mixing (Handique and Burns 2001; Rhee and Burns 2008). With the bidirectional droplet motion, the long displacement distance can be achieved within a limited region instead of through a long channel, thus offering an advantage in conservation of device space. In addition, for convection dominated mixing in our device, the internal recirculation induced by motion in one direction will not be completely reset to the original state when the droplet moves in the opposite direction, because the chamber and channel have different geometry. Therefore, unlike in a uniform channel (Handique and Burns 2001), the bidirectional motion between the chamber and channel works for mixing solutes with low molecular weight (e.g., $D \sim 10^{-5}$ cm^2s^{-1}) even when the mixing is dominated by convection.

3.3 Two-step bioreaction (nested TaqMan® PCR) in droplets

A two-step bioreaction—nested TaqMan® PCR of λDNA— has been chosen to demonstrate the utility of this droplet-based microfluidic platform. Nested TaqMan® PCR involves two successive runs of amplification: the first run is a regular PCR and the second one is a TaqMan® PCR that amplifies a secondary fragment within the first run product. With the two amplification steps, nested TaqMan® PCR can increase the reaction sensitivity and specificity of the overall amplification. The results of both regular TaqMan® PCR and nested TaqMan® PCR conducted in a thermal cycler were shown in Fig. 5. With the same original concentration of template DNA and the same total number of temperature cycles, nested TaqMan® PCR not only increased the fluorescence intensity (i.e., the amplification yield), but also detected target molecules with lower copy number (e.g., 10^2 copies/μL). In contrast, regular TaqMan® PCR was only able to detect template DNA with concentration higher than 10^3 copies/μL.

Nested TaqMan® PCR has also been successfully performed in our droplet-based microsystem. In this experiment, 15 cycles of regular PCR was conducted in the droplet containing the

NIH-PA Author Manuscript

NIH-PA Author Manuscript

NIH-PA Author Manuscript

reaction solution for the first step. Then, another droplet with the same size containing the reagents for the second step was generated, and merged with the first droplet in the chamber. The fluorescence intensity of the merged droplet was monitored in real time through 45 temperature cycles. The results in Fig. 6 show that the fluorescence intensity from the droplet-based regular TaqMan® PCR is barely above the fluorescence threshold even at cycle 45. Since it is not recommended to improve the reaction yield by continuously increasing the number of cycles due to the concern of unspecific products, the droplet-based TaqMan® PCR may be not amenable to detect low copies of target molecules. With the same original concentration of template DNA, the amplification yield in the merged droplet with sufficient mixing is significantly higher than that in the droplet of regular TaqMan® PCR and also higher than that in the merged droplet mixed only by diffusion (Fig. 6). Also, the two-step amplification in the well-mixed droplet is comparable to the off-chip result. The cycle threshold obtained in the well-mixed merged droplet is ~40 cycles earlier than that obtained in the droplet of regular TaqMan® PCR, and ~6 cycles earlier than that obtained in the merged droplet mixed only by diffusion. Therefore, with sufficient on-chip mixing, nested TaqMan® PCR in the droplet-based microsystem can offer faster and more sensitive analysis than regular TaqMan® PCR, especially for detecting low copies of template DNA.

4 Conclusions

We have implemented the generation, merging and mixing of submicroliter-sized droplets on a droplet-based microfluidic platform. In the platform the chamber connected to the three identical droplet-generation channels serves as a compartment not only for merging droplets, but also for carrying out mixing and reaction in the merged droplets. This single multi-functional chamber design offers advantages in conservation of device area and substrate cost. Mixing in the droplet has been characterized with the droplet either staying inside the chamber or moving bidirectionally between the chamber and channel. Both mixing strategies have advantages and disadvantages in practical use. Mixing with the droplet staying in the chamber does not take any additional space. The mixing time is rather long, but it is acceptable for reactions with relatively long reaction time (e.g., DNA amplification). Mixing with the bidirectional droplet motion is much faster, but it requires space in both the chamber and channel, limiting the device flexibility. This mixing strategy is also not amenable for mixing aqueous solution containing surfactant because the interfacial tension will be further reduced with the surfactant already in the oil phase thus significantly reducing the droplet stability.

We have also successfully applied this droplet-based platform to a two-step thermal cycled bioreaction (nested TaqMan® PCR). Our platform can certainly be applied for more complex analyses. In the current design, there are three identical droplet-generation components, so the device can be used to perform droplet-based three-step analyses. One example is the ligation detection reaction (LDR) for detecting single-nucleotide polymorphisms (SNPs), and this analysis includes PCR, protease digestion and ligation reaction with both the PCR and ligation steps requiring temperature cycling.

Supplementary Material

Refer to Web version on PubMed Central for supplementary material.

Acknowledgments

The authors would like to gratefully acknowledge the funding of this work through the grants (5-R01-AI049541-06 and 1-R01-EB006789-01A2) from the National Institutes of Health. The authors would also like to thank the staff and members of the Lurie Nanofabrication Facility (LNF) at University of Michigan for their assistance in device fabrication.

NIH-PA Author Manuscript

NIH-PA Author Manuscript

NIH-PA Author Manuscript

References

Ahmed R, Jones TB. J. Electrost 2006;64:543–549.

Anna SL, Bontoux N, Stone HA. Appl. Phys. Lett 2003;82:364–366.

Avettand-Fènoël V, Chaix M-L, Blanche S, Burgard M, Floch C, Toure K, Allemon M-C, Warszawski J, Rouzioux C. J. Med, Virol 2009;81:217–223. [PubMed: 19107966]

Beer NR, Hindson BJ, Wheeler EK, Hall SB, Rose KA, Kennedy IM, Colston BW. Anal. Chem 2007;79:8471–8475. [PubMed: 17929880]

Beer NR, Wheeler EK, Lee-Houghton L, Watkins N, Nasarabadi S, Hebert N, Leung P, Arnold DW, Bailey CG, Colston BW. Anal. Chem 2008;80:1854–1858. [PubMed: 18278951]

Bringer MR, Gerdts CJ, Song H, Tice JD, Ismagilov RF. Phil. Trans. R. Soc. Lond. A 2004;362:1087–1104.

Chabert M, Viovy J-L. Proc. Natl. Acad. Sci 2008;105:3191–3196. [PubMed: 18316742]

Cho SK, Moon H, Kim C-J. J. Microelectromech, Syst 2003;12:70–80.

Franke T, Abate AR, Weitz DA, Wixforth A. Lab Chip 2009;9:2625–2627. [PubMed: 19704975]

Frenz L, Harrak AE, Pauly M, Bégin-Colin S, Griffiths AD, Baret J-C. Angew. Chem. Int. Ed 2008;47:6817–6820.

Guttenberg Z, Müller H, Habermüller H, Geisbauer A, Pipper J, Felbel J, Kielpinski M, Scriba J, Wixforth A. Lab Chip 2005;5:308–317. [PubMed: 15726207]

Handique K, Burns MA. J. Micromech. Microeng 2001;11:548–554.

Huebner A, Srisa-Art M, Holt D, Abell C, Hollfelder F, deMello AJ, Edel JB. Chem. Commun 2007;12:1218–1220.

Hung L-H, Choi KM, Tseng W-Y, Tan Y-C, Shea KJ, Lee AP. Lab Chip 2006;6:174–178. [PubMed: 16450024]

Jones TB. J. Electrost 2001;51–52:290–299.

Kim S-J, Wang F, Burns MA, Kurabayashi K. Anal. Chem 2009;81:4510–4516. [PubMed: 19419189]

Kumaresan P, Yang CJ, Cronier SA, Blazej RG, Mathies RA. Anal. Chem 2008;80:3522–3529. [PubMed: 18410131]

Lehmann U, Vandevyver C, Parashar VK, Gijs MAM. Angew. Chem. Int. Ed 2006;45:3062–3067.

Link DR, Anna SL, Weitz DA, Stone HA. Phys. Rev. Lett 2004;92:054503-1–054503-4. [PubMed: 14995311]

Mohr S, Zhang Y-H, Macaskill A, Day PJR, Barber RW, Goddard NJ, Emerson DR, Fielden PR. Microfluid Nanofluid 2007;3:611–621.

Niu X, Gulati S, Edel JB, deMello AJ. Lab Chip 2008;8:1837–1841. [PubMed: 18941682]

Ohashi T, Kuyama H, Hanafusa N, Togawa Y. Biomed Microdevices 2007;9:695–702. [PubMed: 17505884]

Paik P, Pamula VK, Pollack MG, Fair RB. Lab Chip 2003;3:28–33. [PubMed: 15100802]

Pal R, Yang M, Lin R, Johnson BN, Srivastava N, Razzacki SZ, Chomistek KJ, Heldsinger D, Haque RM, Ugaz VM, Thwar P, Chen Z, Alfano K, Yim M, Krishnan M, Fuller AO, Larson RG, Burke DT, Burns MA. Lab Chip 2005;5:1024–1032. [PubMed: 16175256]

Pipper J, Inoue M, Ng LF-P, Neuzil P, Zhang Y, Novak L. Nat. Med 2007;13:1259–1263. [PubMed: 17891145]

Pollack MG, Fair RB, Shenderov AD. Appl. Phys. Lett 2000;77:1725–1726.

Pollack MG, Shenderov AD, Fair RB. Lab Chip 2002;2:96–101. [PubMed: 15100841]

Rhee M, Burns MA. Langmuir 2008;24:590–601. [PubMed: 18069861]

Sarrazin F, Prat L, Miceli ND, Cristobal G, Link DR, Weitz DA. Chem. Eng. Sci 2007;62:1042–1048.

Schaerli Y, Wootton RC, Robinson T, Stein V, Dunsby C, Neil MAA, French PMW, deMello AJ, Abell C, Hollfelder F. Anal. Chem 2009;81:302–306. [PubMed: 19055421]

Shestopalov I, Tice JD, Ismagilov RF. Lab Chip 2004;4:316–321. [PubMed: 15269797]

Sivapalasingam S, Patel U, Itri V, Laverty M, Mandaliya K, Valentine F, Essajee S, Trop J. Pediatrics 2007;53:355–358.

Song H, Bringer MR, Tice JD, Gerdts CJ. Appl. Phys. Lett 2003;83:4664–4666. [PubMed: 17940580]

NIH-PA Author Manuscript

NIH-PA Author Manuscript

NIH-PA Author Manuscript

Srinivasan V, Pamula VK, Fair RB. Lab Chip 2004;4:310–315. [PubMed: 15269796]

Srisa-Art M, deMello AJ, Edel JB. Anal. Chem 2007;79:6682–6689. [PubMed: 17676925]

Tan Y-C, Fisher JS, Lee AL, Cristini V, Lee AP. Lab Chip 2004;4:292–298. [PubMed: 15269794]

Tan Y-C, Ho YL, Lee AP. Microfluid Nanofluid 2007;3:495–499.

Thorsen T, Roberts RW, Arnold FH, Quake SR. Phys. Rev. Lett 2001;86:4163–4166. [PubMed: 11328121]

Ting TH, Yap YF, Nguyen N-T, Wong TN, Chai JCK, Yobas L. Appl. Phys. Lett 2006;89:234101–234103.

Um E, Park J-K. Lab Chip 2009;9:207–212. [PubMed: 19107275]

Wang F, Burns MA. Biomed Microdevices 2009;11:1071–1080.

Zheng B, Tice JD, Roach S, Ismagilov RF. Angew. Chem. Int. Ed 2004;43:2508–2511.

NIH-PA Author Manuscript

NIH-PA Author Manuscript

NIH-PA Author Manuscript

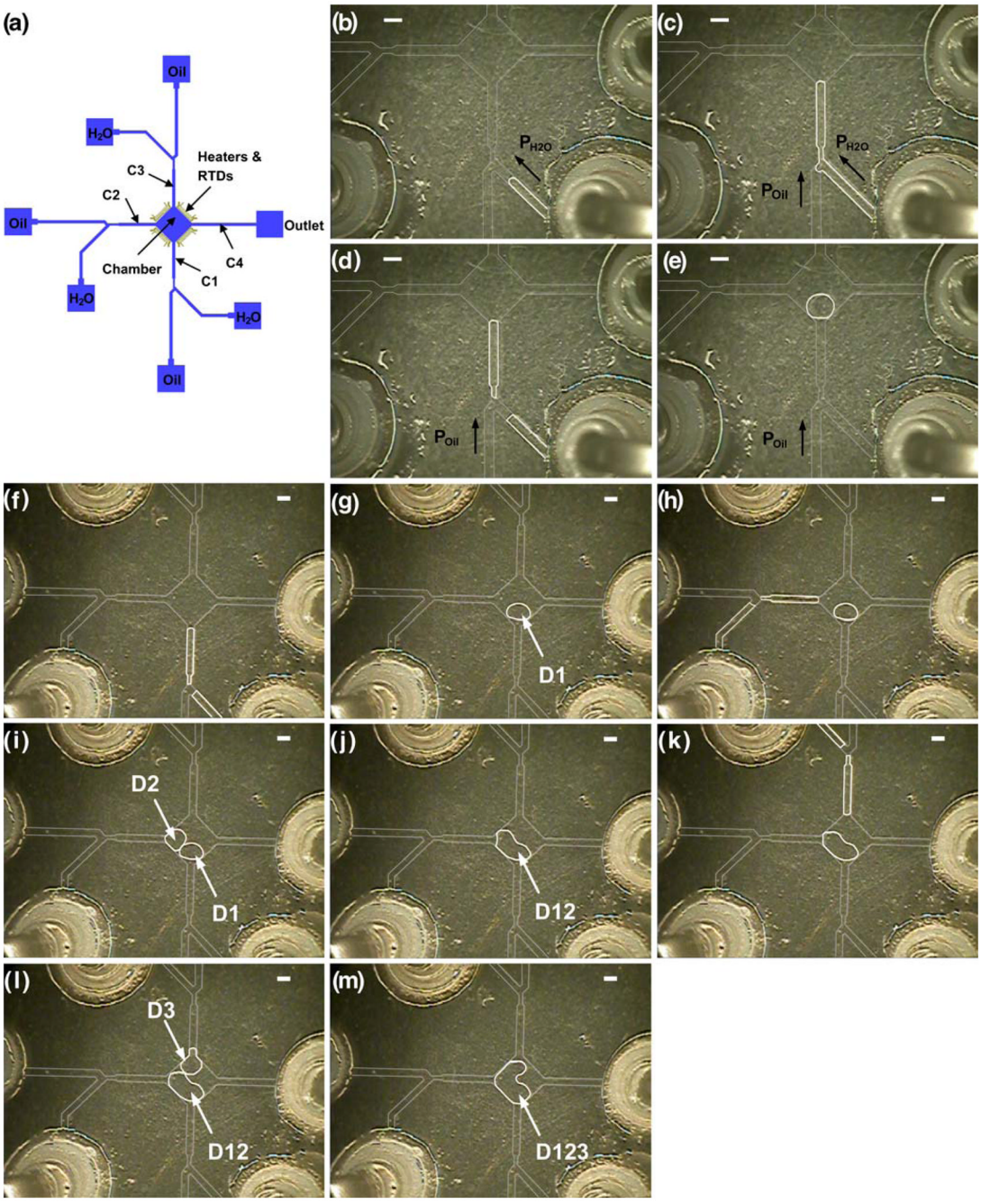

Fig. 1.

(**a**) Schematic of the device design. The four channels connected to the chamber are labeled as C1, C2, C3 and C4, respectively. The four sets of heaters and RTDs are positioned along the edges of the chamber. (**b**)–(**e**) Generation of one droplet. (**f**)–(**m**) Generation and merging of droplets (D1, D2, and D3). The scale bar represents 800 μm

NIH-PA Author Manuscript
NIH-PA Author Manuscript
NIH-PA Author Manuscript

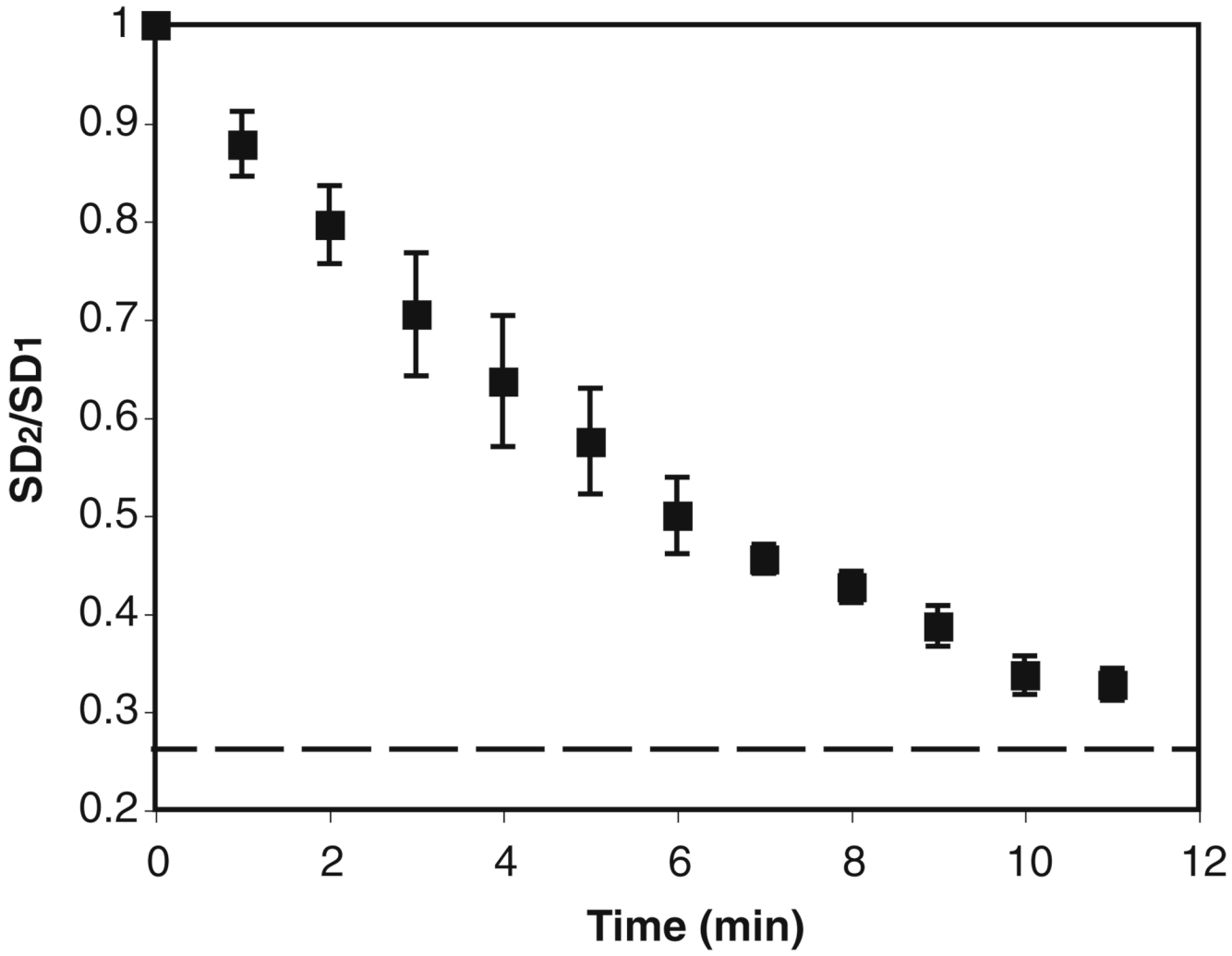

Fig. 2.

Evolution of the standard deviation (SD) of the merged droplet versus time during diffusive mixing. SD_1 is the standard deviation just after the droplet merging. SD_2 is the standard deviation during mixing. The dashed line (SD_2/SD_1=0.259) represents the ratio of the standard deviations between off-chip perfectly mixed and unmixed cases. The error bar represents the standard deviation

NIH-PA Author Manuscript

NIH-PA Author Manuscript

NIH-PA Author Manuscript

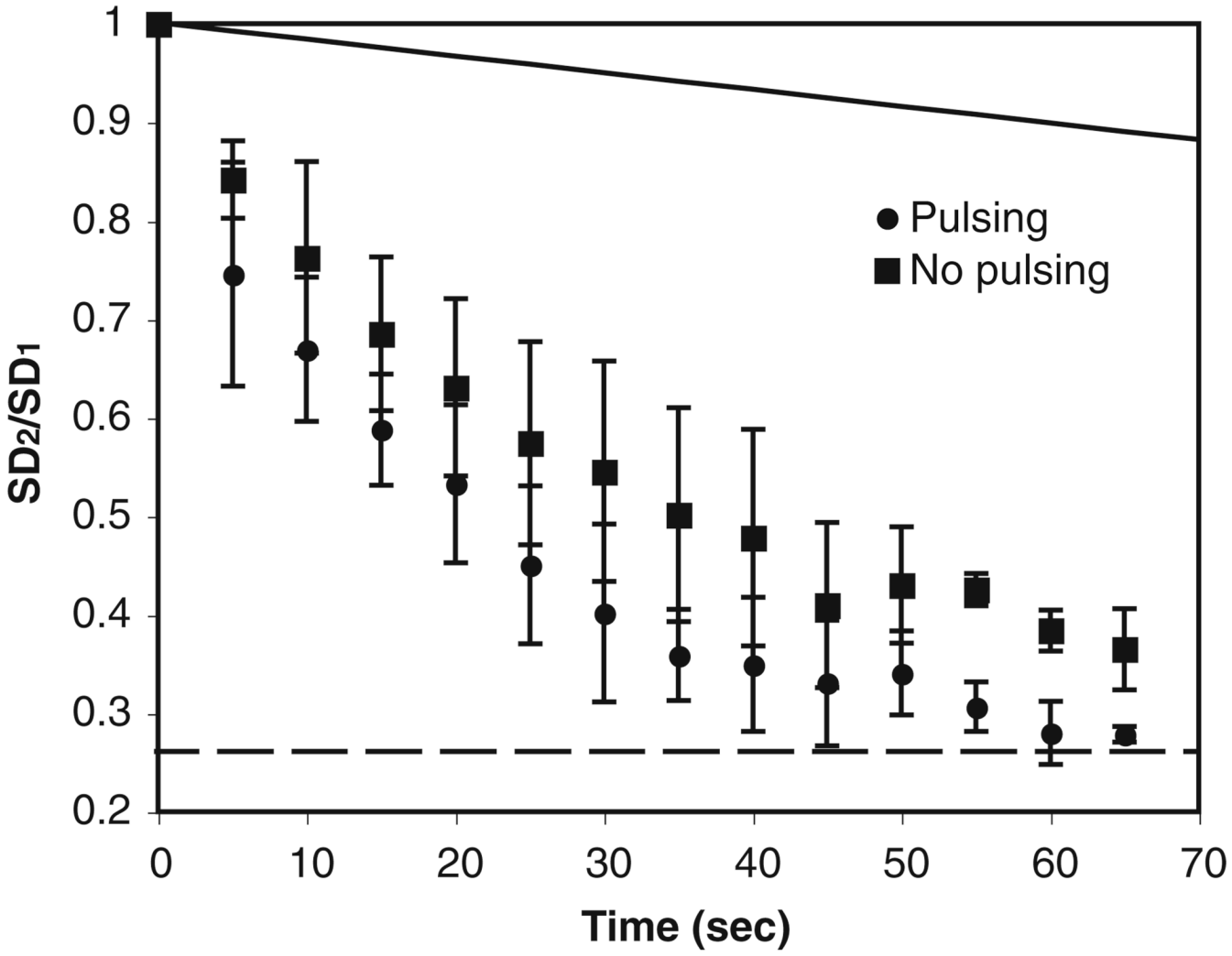

Fig. 3.

Evolution of the standard deviation (SD) of the merged droplet versus time during mixing with the droplet remaining in the chamber. ● Mixing with pulsed pressure; ■ mixing with continuous pressure. The solid line represents the case of diffusive mixing. SD_1, SD_2 and the dashed line are defined in the caption of Fig.2. The error bar represents the standard deviation

NIH-PA Author Manuscript
NIH-PA Author Manuscript
NIH-PA Author Manuscript

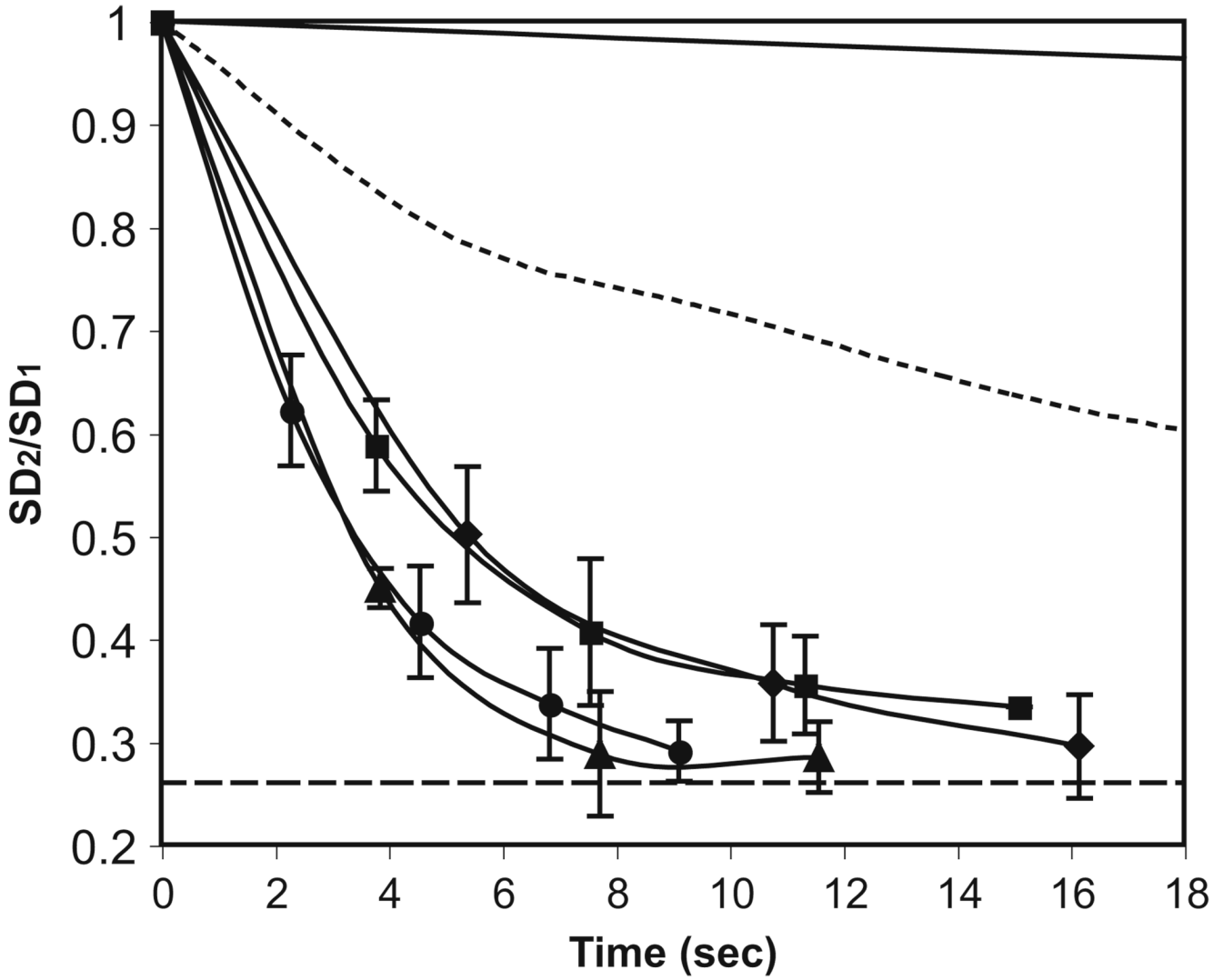

Fig. 4.

Evolution of the standard deviation (SD) of the merged droplet versus time during mixing with the bidirectional droplet motion. The solid line and dotted line represent the cases of diffusive mixing and mixing with droplet in the chamber, respectively. SD_1, SD_2 and the dashed line are defined in the caption of Fig. 2. Each data point was obtained just before the next pulsing cycle. The pulsing parameters are shown in Table 1. Surfactant (Span 80, 0.3% v/v) was added in the oil phase to facilitate the droplet motion without leaving residues on the channel and chamber walls. The error bar represents the standard deviation

NIH-PA Author Manuscript
NIH-PA Author Manuscript
NIH-PA Author Manuscript

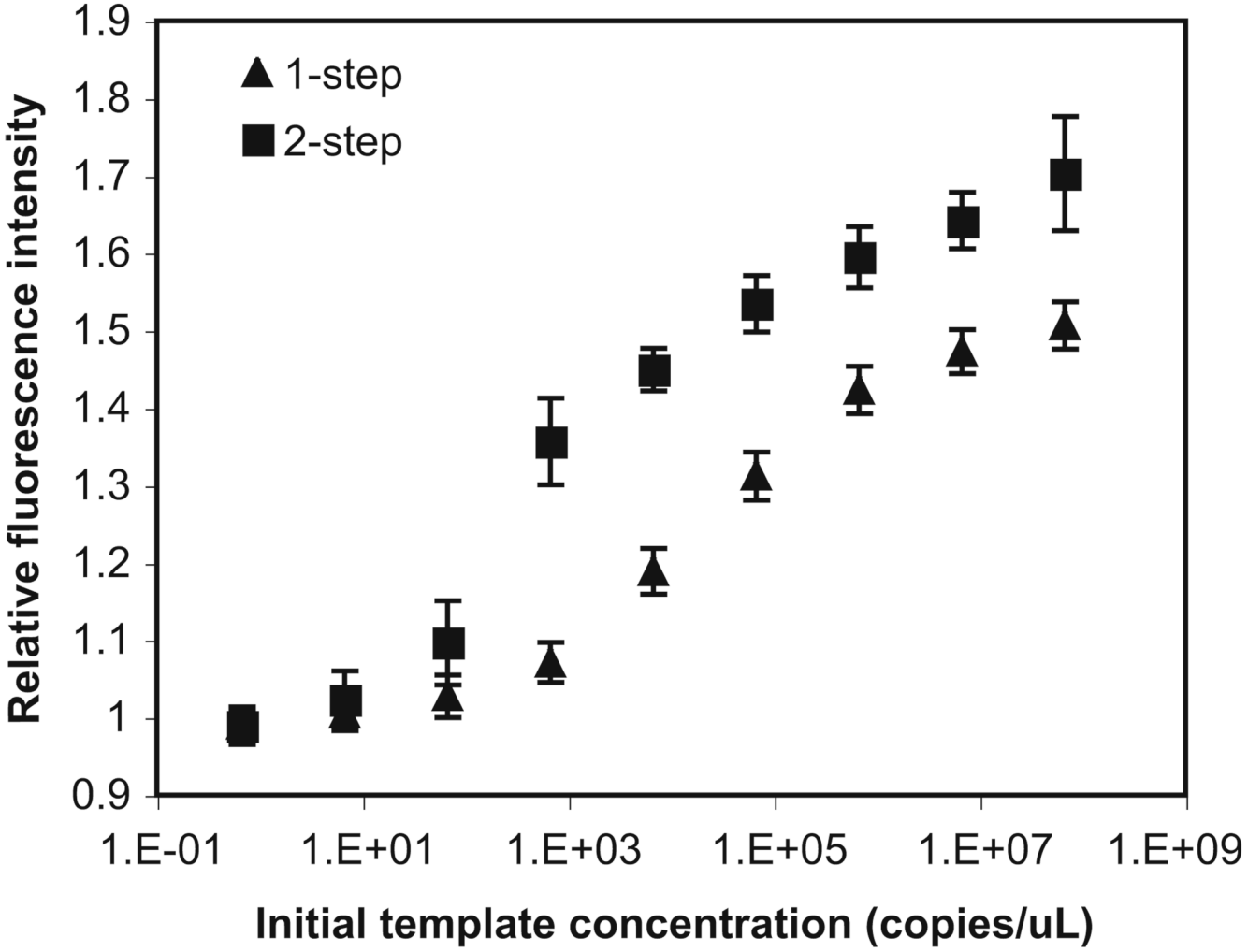

Fig. 5.

Performance of regular TaqMan® PCR (▲) and nested TaqMan® PCR (■) in a thermal cycler. The regular TaqMan® PCR was carried out for 31 cycles. The two steps in nested TaqMan® PCR were carried out for 15 and 16 cycles, respectively. The initial concentration of template λDNA ranges from 3.5 ng/μL (~6.69×10^7 copies/μL) to 3.5×10^{-8}ng/μL (~0.669copies/μL). The reaction volume is 10 μL. The error bar represents the standard deviation

NIH-PA Author Manuscript

NIH-PA Author Manuscript

NIH-PA Author Manuscript

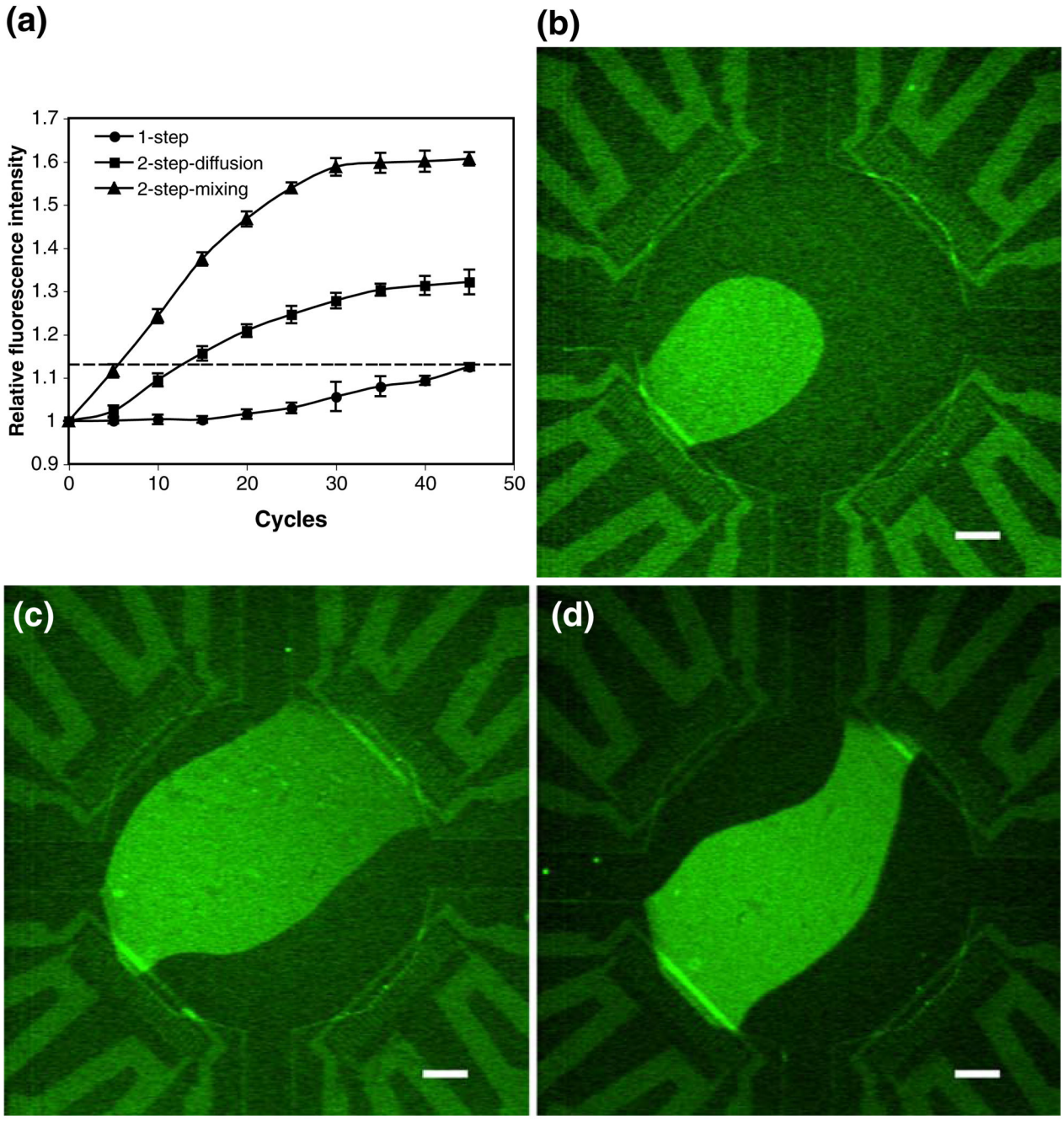

Fig. 6.

(a) Performance of the droplet-based regular TaqMan® PCR (▲) and the nested TaqMan® PCR in a well-mixed droplet (■) and diffusively mixed droplet (●) through 45 cycles. The dashed line represents the fluorescence threshold (1.13). (**b**) Fluorescent image after 31 cycles of regular TaqMan® PCR in a droplet. (**c**)–(**d**) Fluorescent images of nested TaqMan® PCR in a well-mixed and diffusively mixed droplet, respectively. For the images, the two steps in nested TaqMan® PCR were carried out for 15 and 16 cycles, respectively. The original concentration of template λDNA is 3.5×10^{-5} ng/μL (~6.69×10^{2} copies/μL) for both regular and nested TaqMan® PCR. The error bar represents the standard deviation. The scale bar represents 400 μm

NIH-PA Author Manuscript
NIH-PA Author Manuscript
NIH-PA Author Manuscript

Table 1

The pulsing parameters for the applied pressure during mixing with bidirectional droplet motion. ♦, ■, ▲ and ● correspond to the markers in Fig. 4

Pulsing Cycle	Out			In		
	On (ms)	Off (ms)	Times	On (ms)	Off (ms)	Times
♦	20	200	8	40	200	4
■	30	200	4	40	200	4
▲	40	200	4	40	200	4
●	40	100	4	40	100	4